remote sensing

MDPI

Article

A Low-Complexity Underwater Acoustic Coherent Communication System for Small AUV

Weihua Jiang [1,2], Xiaoyu Yang [1,2], Feng Tong [1,2,3,*], Yijun Yang [3] and Tianhua Zhou [4]

[1] Key Laboratory of Underwater Acoustic Communication and Marine Information Technique of the Ministry of Education, Xiamen University, Xiamen 361005, China; whjiang@stu.xmu.edu.cn (W.J.); 22320172201348@stu.xmu.edu.cn (X.Y.)
[2] College of Earth and Ocean Sciences, Xiamen University, Xiamen 361005, China
[3] School of Aerospace Engineering, Xiamen University, Xiamen 361000, China; yangyijun@stu.xmu.edu.cn
[4] Key Laboratory of Space Laser Communication and Detection Technology, Shanghai Institute of Optics and Fine Mechanics, Chinese Academy of Sciences, Shanghai 201800, China; siomzth@siom.ac.cn
* Correspondence: ftong@xmu.edu.cn

Abstract: While underwater acoustic (UWA) communication offers a practical way to establish a wireless link with underwater vehicles, designing a UWA communication system onboard a small autonomous underwater vehicle (AUV) still poses significant challenges. As the adoption of the low-complexity, robust noncoherent communication technology is limited by low bandwidth efficiency and a low data rate, coherent UWA communication requires Doppler mitigation and channel equalization measures to achieve a relatively high data rate in a moving state. Due to the strict constraints of a small-scale AUV in terms of resources and energy consumption, it is not appropriate to use high-complexity Doppler/multipath compensation technology from the prospect of system implementation. In this paper, an efficient and low-complexity UWA differential binary phase-shift keying (DBPSK) system onboard a small AUV is proposed by simplifying the Doppler and multipath compensation. Specifically, for Doppler, the delay of the adjacent DBPSK symbols is calculated according to the Doppler estimate to facilitate delay-tuning Doppler correction. For multipath, low-complexity LMS channel equalization is incorporated with error correction coding to enable multipath mitigation. With a simple structure and low computational complexity, the proposed scheme facilitates the practical hardware implementation and system integration in the small AUV platform. The numerical simulations are conducted to assess the validity of the proposed scheme under different channel conditions and the effectiveness of the proposed scheme is further verified by two UWA communication field tests, which are performed at a practical shallow water sea and lake, respectively.

Keywords: acoustic; underwater acoustic communication; differential modulation; doppler compensation

Citation: Jiang, W.; Yang, X.; Tong, F.; Yang, Y.; Zhou, T. A Low-Complexity Underwater Acoustic Coherent Communication System for Small AUV. *Remote Sens.* **2022**, *14*, 3405. https://doi.org/10.3390/rs14143405

Academic Editors: Songzuo Liu, Nan Chi and Zhi Sun

Received: 8 June 2022
Accepted: 7 July 2022
Published: 15 July 2022

1. Introduction

With the rapid development of marine exploitation, the demand for transmitting data and information has increased significantly [1–3]. As an important carrier for various marine missions, small underwater platforms, such as an autonomous underwater vehicle (AUV), generally with a length smaller than 1.5 m, draw more and more attention from not only the traditional field of environmental monitoring, marine scientific research, and military purpose [4,5] but also the rising personal applications such as underwater sightseeing, self-timers, or entertainment. As a kind of small underwater vehicle, a Micro-sized autonomous underwater vehicle (Micro-AUV) has become a research hotspot due to its small size, low cost, and high flexibility [6,7].

As the adoption of the electromagnetic wave is seriously limited by high attenuation in water medium, the technology of acoustic communication provides an attractive way for Micro-AUVs in underwater control, telemetry, and data transmission [8]. However,

adverse difficulties encountered in a UWA channel, such as multipath, noise, and Doppler, pose a significant challenge to the UWA communication system [1–5]. Moreover, the strictly limited size, power supply, as well as the computational capability provided by a small AUV renders the design of a UWA communication system for a small AUV exceptionally difficult [6–8].

As a noncoherent communication scheme such as MFSK [9] generally cannot meet the need of the data rate for the tremendous application of small AUVs in marine data collection and gathering, coherent strategies draw substantial attention from the research community, a typical choice of which is phase-shift keying (PSK) [10,11]. Compared with an absolute phase-shift keying (PSK) signal, a differential phase-shift keying (DPSK) signal does not need the carrier extraction and is superior in antifrequency drift and phase slow jitter ability. Therefore, DPSK has been recognized as a robust modulation method suitable for low-complexity implementation [12].

For a coherent communication system, the Doppler effect will seriously deteriorate the carrier tracking and phase symbol synchronization of the receiver [13–15], and Doppler estimation and compensation for UWA communication draw extensive attention from the research community. The Doppler value is generally estimated by the correlation calculation between the received signal and multiple copies imposed with a different Dopplers. Then, the received data are resampled according to the Doppler estimation [16–18]. However, the real-time computational complexity associated with the resampling calculation is high. To adapt to the limited capability of a small vehicle, this paper proposed a low-complexity Doppler compensations scheme for DBPSK communication by direct delay tuning.

Specifically, as the physical delay between adjacent DBPSK symbols will be compressed or extended by Doppler, a delay-tuning mechanism is designed to directly compensate the Doppler effects on DBPSK signals. Namely, the delay of DBPSK is calculated according to the Doppler estimate and then used for delay tuning. With the advantages of a simple structure and a low computational complexity, the proposed scheme facilitates easy hardware implementation on board a small vehicle. Moreover, the least mean square (LMS) adaptive equalizer is adopted to reduce the interference of the multipath effect [19,20] with convolutional and interleaving encoding applied to further improve the system performance [21–23]. The numerical simulation as well as the sea and lake trial results verified the effectiveness of the proposed system under a practical shallow water channel.

2. System Principle

2.1. Basic Principle of DBPSK

The DBPSK signal can be described in time domain as [12,24]

$$S_{dbpsk}(t) = b(t) * cos(2\pi f_c t), \tag{1}$$

where f_c is carrier frequency, $b(t)$ is the relative code of the bipolar signal $a(t)$, i.e., $b(t) = a(t) \oplus b(t-1)$. Figure 1 is a block diagram of DBPSK modulation where T_b is the symbol width. DBPSK applies the relative carrier phase of adjacent symbols to represent the digital information. The information transmission of DBPSK signal is realized by the phase difference between the previous and subsequent symbol.

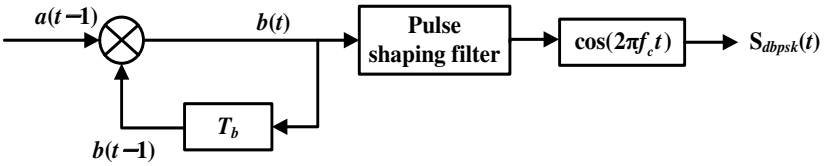

Figure 1. DBPSK modulation.

The differential coherent demodulation method is adopted as shown in Figure 2. The received signal is multiplied by the received signal delayed by one symbol to complete the demodulation. Finally, the judgment sampling is made after lowpass filtering.

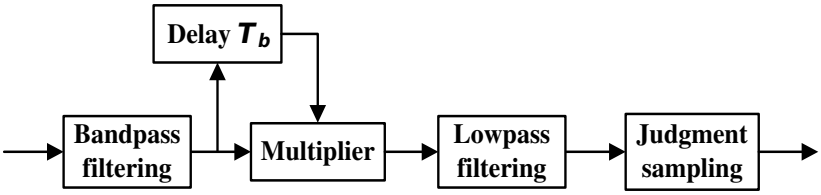

Figure 2. Differential coherence demodulation.

At the receiving end, by the delay multiplication, we have

$$\begin{aligned} x(t) =& S(t) * S(t - T_b) \\ =& b(t) * cos(2\pi f_c t) * b(t - T_b) * cos(2\pi f_c (t - T_b)) \\ =& \frac{1}{2} b(t) * b(t - T_b) * [cos(4\pi f_c t - 2\pi f_c T_b) + cos(2\pi f_c T_b))]. \end{aligned} \tag{2}$$

Therefore, after the lowpass filter, we have

$$y(t) = \frac{1}{2} b(t) * b(t - T_b) * cos(2\pi f_c T_b). \tag{3}$$

2.2. Doppler Estimation and Delay-Tuning Compensation

Considering the Doppler effect on the received signal, the received signal $r(t)$ can be expressed by

$$r(t) = S((1 + \Delta)t), \tag{4}$$

where Δ is the Doppler factor. The Doppler factor Δ can be written as

$$\Delta = \frac{f_d}{f_c}, \tag{5}$$

where f_d is the Doppler frequency offset caused by the relative motion between receiver and transmitter. The main work of Doppler shift compensation includes: (1) Doppler shift estimation. (2) Resampling the received signal, using compression or broadening to recover the signal [13,14].

As the expansion of Doppler in time domain is equivalent to the contraction or expansion degree of signal, the interval between the correlation peaks of linear frequency modulation (LFM) signals is measured for Doppler estimation [25]. Namely, the Doppler factor can be obtained by [13,26]

$$\Delta \approx \frac{T_{rp}}{T_{tp}} - 1, \tag{6}$$

where T_{rp} and T_{tp} are the length of the received signal and the transmitted signal in time domain, respectively.

In this paper, a direct delay-tuning Doppler compensation scheme is proposed for differential demodulation. For the demodulation, the delay T_s is applied to adjacent DBPSK symbols. Therefore, by the delay multiplication, the signal $x(t)$ is shown as

$$\begin{aligned} x(t) =& S((1 + \Delta)t) * S[(1 + \Delta)(t - T_b + T_s)] \\ =& b((1 + \Delta)t) * b[(1 + \Delta)(t - T_b + T_s)] * \\ & cos(2\pi(f_c + f_d)t) * cos(2\pi(f_c + f_d)(t - T_b + T_s)) \\ =& \frac{1}{2} b((1 + \Delta)t) * b[(1 + \Delta)(t - T_b + T_s)] * \\ & \{cos[4\pi(f_c + f_d)t - 2\pi(f_c + f_d)(T_b - T_s)] + cos[2\pi(f_c + f_d)(T_b - T_s)]\}. \end{aligned} \tag{7}$$

Then, after the lowpass filtering, we have

$$y(t) = \frac{1}{2} b((1+\Delta)t) * b[(1+\Delta)(t - T_b + T_s)] * cos[2\pi(f_c + f_d)(T_b - T_s)]. \quad (8)$$

Therefore, to remove the effect of Doppler shift, let

$$(1+\Delta)t - (1+\Delta)(t - T_b + T_s) = T_b, \quad (9)$$

$$(f_c + f_d)(T_b - T_s) = f_c T_b. \quad (10)$$

We assume that a Doppler f_d is estimated. We solve (9) and (10), the delay between adjacent DBPSK symbols associated with Doppler f_d can be expressed by

$$T_s = \frac{f_d T_b}{f_c + f_d}, \quad (11)$$

where T_s is the delay between adjacent DBPSK symbols, T_b is the symbol width, and f_d is the estimated Doppler.

Doppler compensation can be carried out through the delay of the received signal to offset the frequency offset caused by Doppler effect and improve the performance of UWA communication. This scheme is suitable for the real-time processing of UWA communication system.

For the signal with N sampling points, while the computational complexity of resampling method is $\mathcal{O}(N^2)$ [27], the complexity of the delay-tuning method is only one multiplication, one addition, and one division, i.e., calculation of parameter T_s. Thus, the proposed delay-tuning method leads to significant computational complexity saving.

2.3. UWA Communication System

Figure 3 shows the flow chart of UWA communication system. At the transmitting side, the transmitted data are coded by differential coding, and then convolution encoding and interleaving encoding are performed. The encoded data are modulated by DBPSK, and the modulated signal is transmitted to the UWA channel through the transducer. At the receiving side, the received signal is firstly processed by the bandpass filter. Secondly, the Doppler estimation is carried out to facilitate the direct delay-tuning compensation as mentioned in Section 2.2. Then, the delay multiplication is performed, and goes through the lowpass filter. Afterward, the LMS equalizer, as well as interleaving decoding and convolution decoding, is applied to reduce the multipath effect and burst errors. Finally, the original data are restored and output. Specifically, in the proposed UWA communication system, the signal in the frequency ranges from 13 to 18 kHz, and a 2.5 kHz lowpass filter is implemented to remove the high-frequency components, leaving only a baseband signal, as shown in (3).

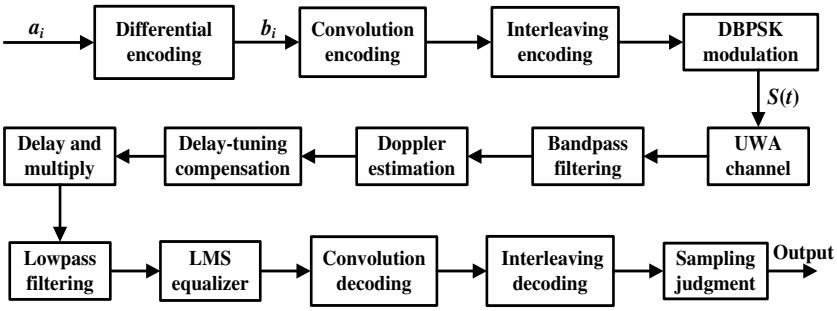

Figure 3. System flow diagram.

Based on STM32F407 processor, UWA communication system for Micro-AUV is designed. The hardware module of UWA communication system is mainly composed of upper computer, STM32F407 processor, and signal processing circuit, as shown in Figure 4.

The core modulation and demodulation program of UWA communication system mainly includes three modules: serial communication module, transmitting module, and receiving module. The serial interface module is used for communication between the processor and the host computer, which can receive the control information from the host computer and upload the current system status. For the transmitting module, a power amplifier is applied to carry out the piezoelectric transducer excitation and the power of transmitter can reach 50 Watt. Moreover, at the receiving end, the AD603 chip and MAX274 chip are applied to preamplify the signal received by hydrophone and filter the out-of-band noise, respectively. The bandpass filter is designed with a central frequency of 15,500 Hz and a bandwidth of 5000 Hz. The sampling frequency of analog to digital converters (ADC) is configured as 75 kHz.

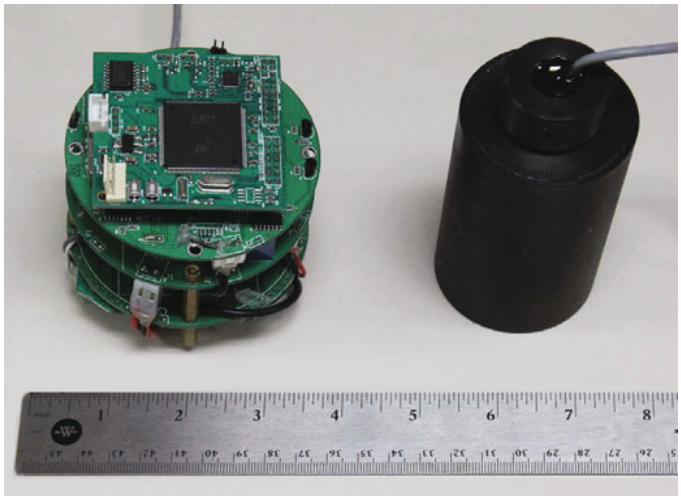

Figure 4. The UWA communication system.

3. Numerical Simulation

To further verify the effectiveness of the proposed communication scheme, a numerical simulation is performed. We used the bell-hop toolkit [28] to generate the simulation channels. The desired signal is generated by adding the Gaussian noise, and the signal-to-noise ratio (SNR) of the received signal is assumed to be 15 dB with a communication distance of 1000 m. In addition, the LMS equalizer is adopted to reduce the interference of the multipath effect. The primary simulation parameters are presented in Table 1. We also change some of the parameters in Table 1 to test the performance of the proposed scheme under different communication conditions, which will be mentioned below. In our numerical simulation, bit error rate (BER) is applied to the performance evaluation of different algorithms. The BER is defined as the number of bits received in error divided by the total number of bits received.

We start by examining the performance of the proposed scheme under different SNRs. The BER outputs of different communication schemes under different SNRs with a Doppler of -8 Hz are shown in Figure 5. Comparing the results for three schemes, we note that the results of the scheme without compensation fall much lower due to the Doppler shift and the noise. The proposed delay-tuning Doppler compensation scheme obtains a similar performance to the resampling Doppler compensation scheme at high SNR conditions, while the proposed scheme achieves the best BER results for low SNR events. Although the resampling Doppler compensation scheme can effectively eliminate the Doppler shift, the noise can affect the resampling accuracy.

Next, to investigate the performance under different Doppler conditions, Figure 6 shows the BER results under different Dopplers at an SNR of 15dB. We observe that the BER performance degrades as the Doppler increases, particularly for the scheme without compensation. After Doppler compensation, the resampling Doppler compensation scheme and the proposed scheme obtain substantial BER performance improvement. With a lower

computational complexity, the proposed scheme achieves a BER performance that is less than 2%, even at Doppler = −10 Hz. Thus, the numerical evaluation indicates that the proposed delay-tuning method is capable of compensating the Doppler shift at the expense of low computational complexity.

Table 1. The primary simulation parameters.

Description	Value
Carrier frequency	15,500 Hz
Sampling frequency	96,000 Hz
Bandwidth	5000 Hz
Data rate	2000 bps
Communication distance	1000 m
Water depth	40 m
SNR	15 dB
Receiver depth	10 m
Transmitter depth	10 m
Doppler	−8 Hz
Known symbols for training	200 bits
Unknown data symbols for recovering	1800 bits
Order of LMS filter	120
Step factor of LMS equalizer	0.01
Iteration number	10,000

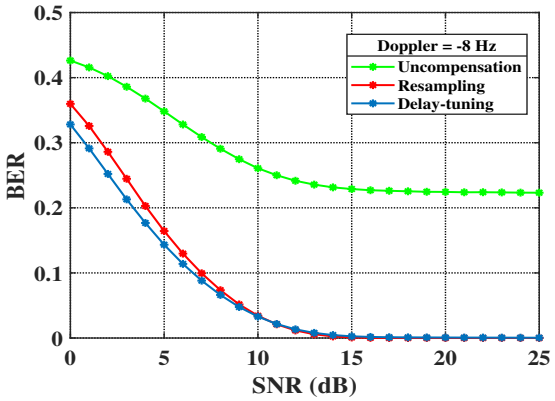

Figure 5. The BER outputs of different communication schemes under different SNR at Doppler = −8 Hz.

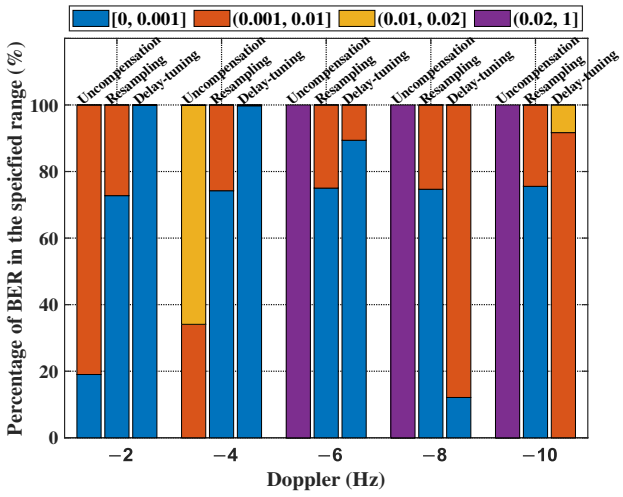

Figure 6. The BER outputs of different communication schemes under different Doppler conditions.

Next, in Figure 7, we show the results for data rate values ranging between 1000 and 3000 bps. We observe an expected performance decrease as the data rate increases. Comparing the results for the scheme without compensation, we note that the resampling Doppler compensation scheme and the proposed delay-tuning Doppler compensation scheme achieve the results with an average reduction of 10.4 and 10.1% in BER, respectively. In particular, the proposed scheme can work well with a high data rate because most BER values of the proposed scheme are less than 1%.

Next, to investigate the performance under the different receiver depth conditions, we set the receiver depth to 5, 10, 15, 20, and 25 m, respectively, with a water depth of 40 m. Figure 8 shows the BER results for different receiver depths at SNR = 15 dB. We observe that the BER performance of the three communication schemes is greatly affected by the different channel structure under the different receiver depth conditions. However, because the LMS equalizer can effectively suppress the multipath effect, the proposed scheme and the resampling Doppler compensation scheme can obviously improve the communication performance with Doppler compensation. Moreover, compared to the resampling Doppler compensation scheme, the proposed scheme achieves a slightly worse performance and a BER of less than 2% with a much lower computational cost.

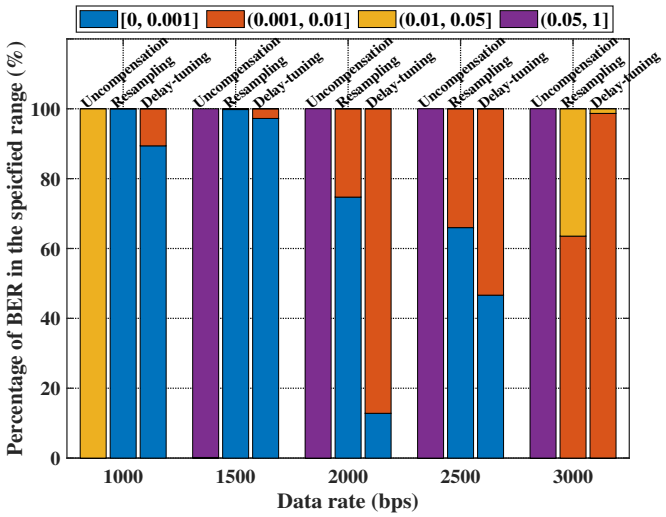

Figure 7. The BER outputs of different communication schemes under different data rate conditions at Doppler = −8 Hz.

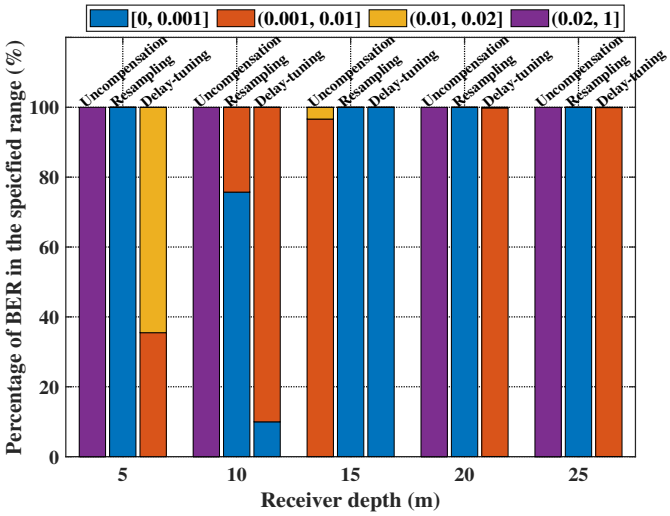

Figure 8. The BER outputs of different communication schemes under different receiver depth conditions at Doppler = −8 Hz.

Finally, we investigate the performance under the different carrier conditions. Because the absorption of sound in sea water varies markedly with frequency [29], according to the absorption factor and the SNR value for a carrier frequency of 15.5 kHz, we assume that the carrier frequencies of 5, 10, 20, 30, and 40 kHz correspond to an SNR of the received signals of 17, 16, 13, 10, and 5 dB, respectively. Figure 9 shows a histogram for the BER as obtained under the different carrier conditions. Due to the influence of a low SNR, three communication schemes do not perform well at high frequencies. At low frequencies, however, the proposed delay-tuning Doppler compensation scheme performs significantly better than the scheme without compensation.

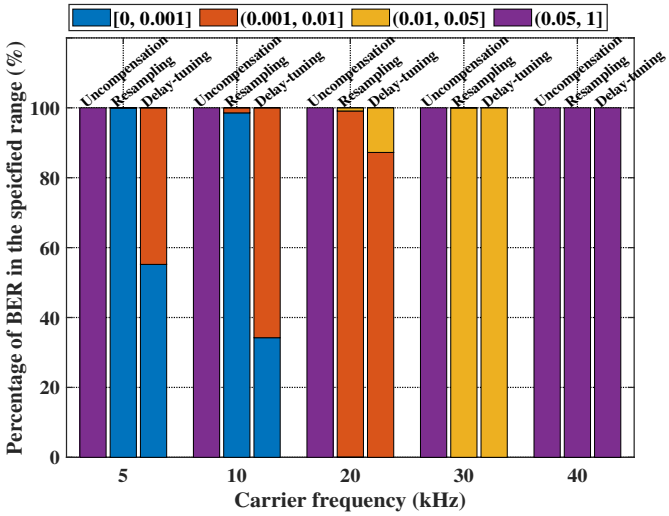

Figure 9. The BER outputs of different communication schemes under different carrier frequency conditions at Doppler = −8 Hz.

4. Experiments and Discussions

4.1. Sea Experiment

In order to verify the proposed communication scheme, the sea trial was carried out in Xiamen port, China, on 11 May 2017. The water depth of the experimental area is about 10 m. The UWA communication system of the experiment includes one transmitter and one receiver. The transmitter and the receiver are located at 4 m underwater. The distance between the transmitter and the receiver is 500 m. We used the HY1203 sound velocity profiler to measure the underwater sound velocity at different water depths [30]. The setup of the field experiment and the corresponding sound velocity profile are shown in Figure 10. In the experiment, the transmitting ship is anchored and the receiving ship drifts with the current, as displayed in Figure 10a, to simulate the mobile communication scenario of an AUV. The resulting Doppler is approximately −2.5 Hz, corresponding to a Doppler factor of -1.67×10^{-4}, and the SNR of the received signal is 10 dB.

The parameters of the DBPSK modulation and demodulation are given as follows. With a sampling rate of 75 kHz and a carrier frequency of 15 kHz, the bandwidth is 13–18 kHz. The effective data rate is 1172 bps. The synchronization sequence adopts an LFM signal with a frequency from 13 to 18 kHz. The frame structure of the DBPSK signal is shown in Figure 11. The transmit packet is composed of a synchronization sequence, protection interval, training symbols, and data symbols. To estimate the Doppler shift, the correlation detection between an LFM preamble and an LFM postamble around each data frame is performed to obtain the variation of the time difference between the first and last correlation peaks, which can be transformed into the Doppler factor [18,31].

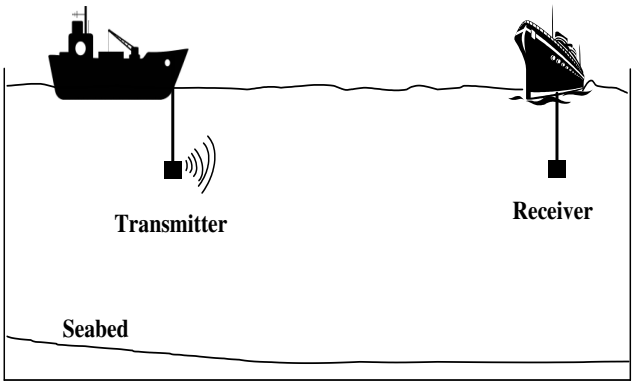

(**a**)

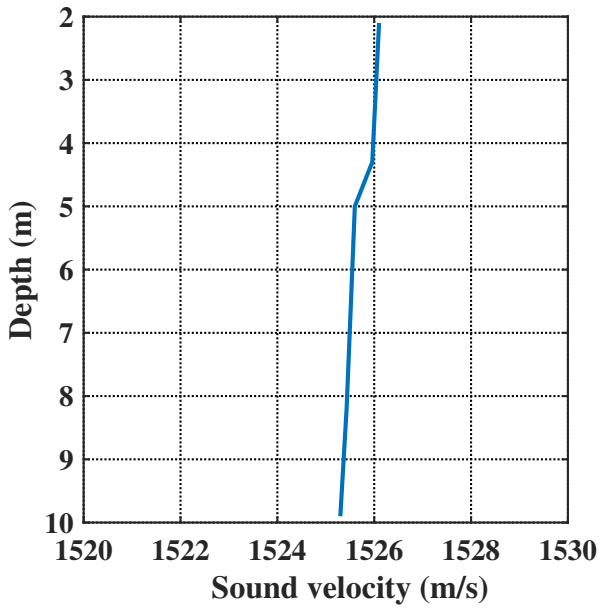

(**b**)

Figure 10. Setup of the field experiment and the corresponding sound velocity profile. (**a**) Setup of the field experiment. (**b**) Sound velocity profile.

LFM	Guard time	Training symbols (200)	Information symbols (420)	Guard time	LFM
50ms	200ms			200ms	50ms

Figure 11. The frame format of DBPSK signal.

As the typical multipath spread of the UWA channels may be in the order of tens of milliseconds, the length of the protection interval and training sequence are set to 200 ms and 200 symbols, respectively, as displayed in Figure 11. Note that the multipath spread of the two experimental UWA channels as presented below in Figures 12 and 15 are both within ten milliseconds. In addition, the (2, 1, 7) convolutional code is adopted, and the generating polynomial of the convolutional code is (171, 133). A Viterbi decoder uses the Viterbi algorithm for convolution decoding. The interleaving depth is 7 bits for the interleaving encoding. For the LMS equalizer, 200 known symbols are used for LMS equalizer training. The step factor of the LMS equalizer is 0.01, and the order of the filter is 20.

Figure 12 shows the channel impulse response (CIR) of the experiment channel, which reveals that there exists a typical multipath structure. As the LMS equalizer is designed for

canceling the multipath interference (ISI) induced by the multipath effect, the experimental channel as shown in Figure 12 provides an effective approach to quantitatively assess the performance of the proposed communication system.

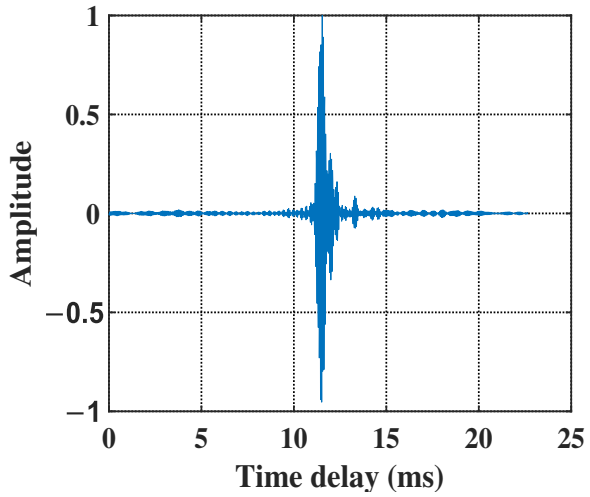

Figure 12. The CIR of the experiment channel.

In our experiment, BER and output signal-to-noise ratio (*OSNR*) are applied to the performance evaluation of different algorithms. *OSNR* is defined by [32,33]

$$OSNR = 10\log_{10}\frac{\|\mathbf{s}\|_2^2}{\|\mathbf{s}-\tilde{\mathbf{s}}\|_2^2}, \tag{12}$$

where $\mathbf{s}$ is the transmitted symbol, and $\tilde{\mathbf{s}}$ is the soft output from the receiver. In order to test the anti-Doppler communication performance of the proposed method, the experimental results of three schemes without Doppler compensation, resampling Doppler compensation, and delay-tuning Doppler compensation are compared.

Table 2 shows the BER and *OSNR* of the sea trial under different communication schemes and also provides the BER and *OSNR* results at uncoded and coded conditions. It can be seen from Table 2 that, while the scheme without Doppler compensation achieves the worst BER and *OSNR* results among the three types of receivers, both the resampling Doppler compensation and delay-tuning compensation yield a significant improvement in BER and *OSNR* behavior. Note that with a significantly lower computational complexity, the proposed delay-tuning strategy corresponds to a slightly worse performance than the resampling compensation does, i.e., 4.34% with respect to 4.19% in the uncoded BER, 21.18 dB with respect to 21.40 dB in the coded *OSNR*.

Table 3 shows the coded BER and *OSNR* output under different communication schemes at unequalization and LMS equalizer conditions. As provided in Table 3, compared with the unequalization scenario, the LMS equalizer can effectively suppress the multipath effect and obviously improve the communication performance for three different Doppler compensation schemes.

Table 2. BER and *OSNR* under different communication schemes with LMS equalizer at uncoded and coded conditions for sea experiment.

Scheme	BER (%)		*OSNR* (dB)	
	Uncoded	Coded	Uncoded	Coded
Uncompensation	12.58	15.46	5.92	3.49
Resampling compensation	4.19	0.10	10.68	21.40
Delay-tuning compensation	4.35	0.26	10.52	21.18

Table 3. The coded BER and *OSNR* under different communication schemes at unequalization and LMS equalizer conditions for sea experiment.

Scheme	BER (%)		*OSNR* (dB)	
	Unequalization	LMS	Unequalization	LMS
Uncompensation	20.17	15.46	1.78	3.49
Resampling compensation	0.23	0.10	19.95	21.40
Delay-tuning compensation	0.41	0.26	20.12	21.18

Similarly, from the constellation given in Figure 13, one may observe that the receiver with delay-tuning Doppler compensation or resampling compensation obviously outperforms that without Doppler compensation, with the corresponding constellations exhibiting a better separation pattern than that of the latter.

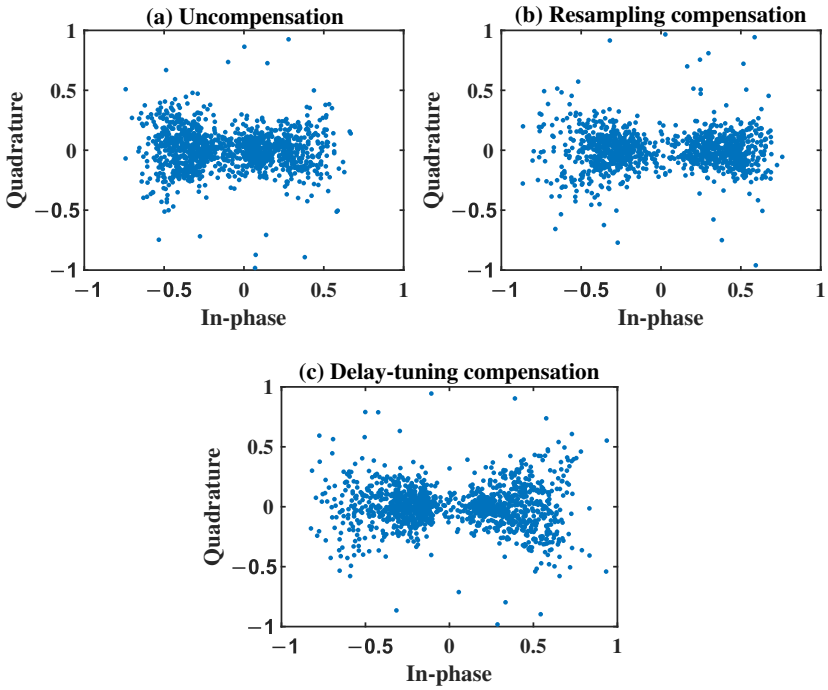

Figure 13. The uncoded constellation under different communication schemes of the sea experiment.

Next, to examine the performance of the proposed scheme under the different Doppler conditions for the sea experiment, we explored the results by using sea experimental data in an emulation framework. That is, the recorded signal is resampled to a target Doppler value. Figure 14 shows the BER results for Doppler shift values ranging between −3 and −15 Hz. We observe that compared to without Doppler compensation, the resampling Doppler compensation scheme and the proposed scheme achieve a significant improvement in the BER performance. While the resampling Doppler compensation scheme gives the best results, the proposed scheme also yields excellent results and achieves a BER of 2.6%, even at Doppler = −15 Hz. Thus, it can be concluded that the delay-turning Doppler compensation method is capable of achieving a similar compensation effect as the conventional resampling compensation, with a much lower computational complexity.

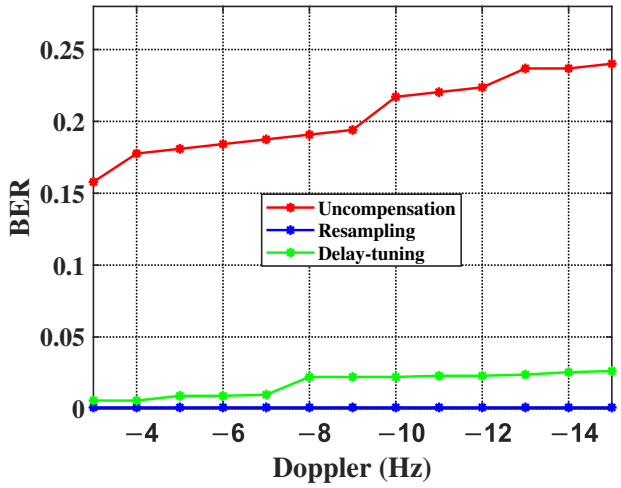

Figure 14. The BER outputs of different communication schemes under different Doppler conditions for sea experimental data.

4.2. Lake Experiment

The lake experiment was performed in Fuxian Lake, China, on 11 November 2020. The water depth of the experimental area is about 40 m. The UWA communication system is one transmitter and one receiver. The transmitter and the receiver are located at 5 and 10 m underwater, respectively. The distance between the transmitter and the receiver is 600 m. The setup of the experiment is shown in Figure 10. In the experiment, both the transmitting ship and receiving ship drift with the current, corresponding to a Doppler of about -1 Hz and a Doppler factor of 6.67×10^{-5}. The SNR of the received signal is 15 dB. In Figure 15, the CIR of the lake experimental channel is presented, which corresponds to a multipath spread of about 3 ms due to the closed lake environment.

Table 4 shows the BER and *OSNR* under different communication schemes. As described in Table 4, for the uncoded and coded scenarios, the receiver without any Doppler compensation corresponds to the worst BER and *OSNR* performances. One may also observe that both the resampling and delay-tuning Doppler compensation significantly improved the BER and *OSNR* of communication. Moreover, the performance is further enhanced by applying encoding. Table 5 shows the results obtained in the unequalization and LMS equalizer scenarios, from which the performance enhancement achieved by the LMS equalizer is evident.

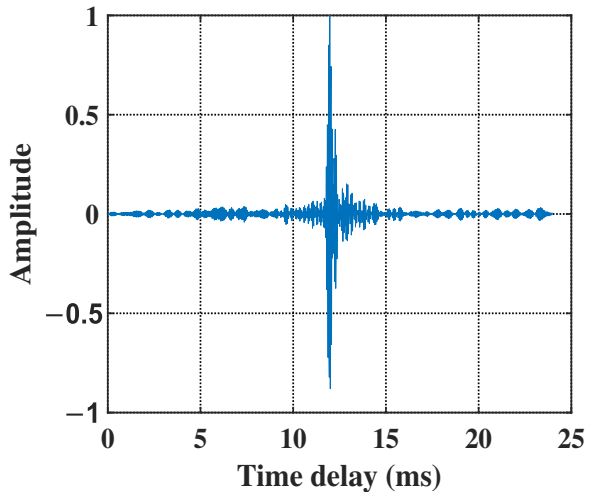

Figure 15. The CIR of the lake experiment channel.

Table 4. BER and *OSNR* under different communication schemes with LMS equalizer at uncoded and coded conditions for lake experiment.

Scheme	BER (%)		*OSNR* (dB)	
	Uncoded	Coded	Uncoded	Coded
Uncompensation	11.32	0.53	4.64	11.86
Resampling compensation	1.37	0.08	18.09	21.58
Delay-tuning compensation	1.49	0.11	18.43	21.74

Table 5. The coded BER and *OSNR* under different communication schemes at unequalization and LMS equalizer conditions for lake experiment.

Scheme	BER (%)		*OSNR* (dB)	
	Unequalization	LMS	Unequalization	LMS
Uncompensation	9.40	0.53	5.51	11.86
Resampling compensation	0.17	0.08	20.29	21.58
Delay-tuning compensation	0.24	0.11	20.61	21.74

Figure 16 shows the constellation of different communication schemes. Specifically, the constellation obtained by the receiver without the Doppler compensation scheme is the worst, with many constellation points falling into the incorrect boundary, while the constellation obtained by the resampling compensation and delay-tuning compensation scheme yield better separation effects. In conclusion, both the sea and lake experiment results demonstrate the effectiveness of the proposed method.

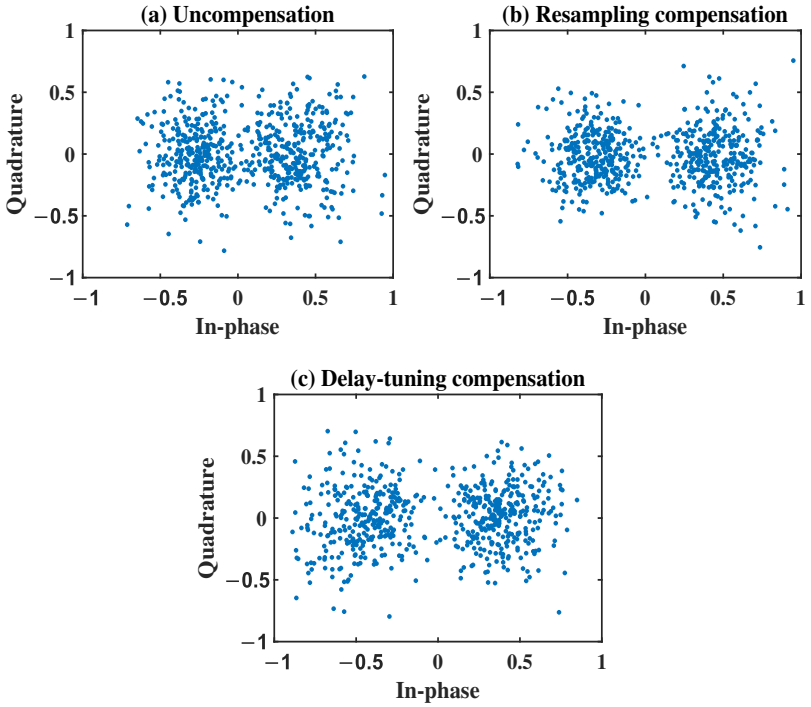

Figure 16. The uncoded constellation under different communication schemes of the lake experiment.

5. Conclusions

Due to the multipath effect and Doppler shift of a UWA channel, the performance of a coherent UWA communication system will be seriously degraded. Meanwhile, for a UWA communication system onboard small AUVs, the limitation of low complexity and limited computational capability pose significant challenges.

In this paper, a DBPSK acoustic communication system is designed for a small AUV purpose by incorporating the delay-tuning Doppler compensation approach with LMS equalization to enable low-complexity Doppler and multipath suppression. Channel encoding and interleaving are further adopted to guarantee the communication performance.

The numerical simulation is carried out to comprehensively analyze the performance of the proposed scheme under different SNR, Doppler shift, data rate, receiver depth, and carrier frequency conditions. Moreover, the sea trial and lake experiment results demonstrated the effectiveness of the proposed system in achieving reliable communication behavior at the expense of low complexity. Future work will include the integration and performance evaluation of the proposed underwater acoustic coherent communication system on the practical small AUV platform [8].

Author Contributions: Conceptualization, F.T.; Data curation, W.J. and X.Y.; Investigation, W.J. and X.Y.; Methodology, F.T. and T.Z.; Software, W.J., X.Y., F.T. and Y.Y.; Validation, W.J. and T.Z.; Writing—original draft, W.J.; Writing—review & editing, F.T. All authors have read and agreed to the published version of the manuscript.

Funding: This research was funded by the National Key Research and Development Program of China (No.2018YFE0110000), the CAS Strategic Leading Science and Technology Project Category A (No.XDA22000000), and the Key Program of National Natural Science Foundation (No.62031011).

Data Availability Statement: The data presented in this paper are available after contacting the corresponding author.

Conflicts of Interest: The authors declare no conflict of interest.

References

1. Li, J.; Bai, Y.; Zhang, Y.; Qu, F.; Wei, Y.; Wang, J. Cross power spectral density based beamforming for underwater acoustic communications. *Ocean Eng.* **2020**, *216*, 107786. [CrossRef]
2. Huang, J.; Diamant, R. Adaptive Modulation for Long-Range Underwater Acoustic Communication. *IEEE Trans. Wirel. Commun.* **2020**, *19*, 6844–6857. [CrossRef]
3. Wu, F.Y.; Yang, K.; Duan, R. Compressed Sensing of Underwater Acoustic Signals via Structured Approximation l_0-Norm. *IEEE Trans. Veh. Technol.* **2018**, *67*, 8504–8513. [CrossRef]
4. Zhang, D.; N'Doye, I.; Ballal, T.; Al-Naffouri, T.Y.; Alouini, M.S.; Laleg-Kirati, T.M. Localization and Tracking Control Using Hybrid Acoustic–Optical Communication for Autonomous Underwater Vehicles. *IEEE Internet Things J.* **2020**, *7*, 10048–10060. [CrossRef]
5. Han, X.; Yin, J.; Tian, Y.; Sheng, X. Underwater acoustic communication to an unmanned underwater vehicle with a compact vector sensor array. *Ocean Eng.* **2019**, *184*, 85–90. [CrossRef]
6. Duecker, D.A.; Steinmetz, F.; Kreuzer, E.; Renner, C. Micro AUV Localization for Agile Navigation with Low-cost Acoustic Modems. In Proceedings of the 2020 IEEE/OES Autonomous Underwater Vehicles Symposium (AUV) (50043), St. Johns, NL, Canada, 30 September–2 October 2020; pp. 1–7.
7. Eldred, R.; Lussier, J.; Pollman, A. Design and Testing of a Spherical Autonomous Underwater Vehicle for Shipwreck Interior Exploration. *J. Mar. Sci. Eng.* **2021**, *9*, 320. [CrossRef]
8. Tao, Q.y.; Zhou, Y.h.; Tong, F.; Song, A.j.; Zhang, F. Evaluating acousticcommunication performance of micro autonomous underwater vehicles in confined spaces. *Front. Inf. Technol. Electron. Eng.* **2018**, *19*, 1013–1023. [CrossRef]
9. Cao, X.L.; Jiang, W.H.; Tong, F. Time reversal mfsk acoustic communication in underwater channel with large multipath spread. *Ocean Eng.* **2018**, *152*, 203–209. [CrossRef]
10. Stojanovic, M. Recent advances in high-speed underwater acoustic communications. *IEEE J. Ocean. Eng.* **1996**, *21*, 125–136. [CrossRef]
11. He, C.; Zhang, Q.; Yan, Z.; Li, Q.; Zhang, L.; Chen, J.; Qi, Q. Experimental demonstration of phase-coherent underwater acoustic communications using a compact array. *Ocean Eng.* **2017**, *145*, 207–214. [CrossRef]
12. Stojanovic, M. An adaptive algorithm for differentially coherent detection in the presence of intersymbol interference. *IEEE J. Sel. Areas Commun.* **2005**, *23*, 1884–1890. [CrossRef]
13. Li, B.; Zheng, S.; Tong, F. Bit-error rate based Doppler estimation for shallow water acoustic OFDM communication. *Ocean Eng.* **2019**, *182*, 203–210. [CrossRef]
14. Han, J.; Chepuri, S.P.; Leus, G. Joint channel and Doppler estimation for OSDM underwater acoustic communications. *Signal Process.* **2020**, *170*, 107446. [CrossRef]
15. Stojanovic, M. Underwater acoustic communication. In *Wiley Encyclopedia of Electrical and Electronics Engineering*; John Wiley & Sons, Inc.: New York, NY, USA, 1999; pp. 1–12.

16. Qu, F.; Wang, Z.; Yang, L.; Wu, Z. A journey toward modeling and resolving doppler in underwater acoustic communications. *IEEE Commun. Mag.* **2016**, *54*, 49–55. [CrossRef]
17. Li, B.; Zhou, S.; Stojanovic, M.; Freitag, L.; Willett, P. Multicarrier communication over underwater acoustic channels with nonuniform Doppler shifts. *IEEE J. Ocean. Eng.* **2008**, *33*, 198–209.
18. Sharif, B.S.; Neasham, J.; Hinton, O.R.; Adams, A.E. A computationally efficient Doppler compensation system for underwater acoustic communications. *IEEE J. Ocean. Eng.* **2000**, *25*, 52–61. [CrossRef]
19. Pelekanakis, K.; Chitre, M. Comparison of sparse adaptive filters for underwater acoustic channel equalization/estimation. In Proceedings of the 2010 IEEE International Conference on Communication Systems, Singapore, 17–19 November 2010; pp. 395–399.
20. Zheng, Y.; Hao, X.; Yan, X. New least mean square algorithm with variable step based on underwater acoustic communication. *J. Comput. Appl.* **2017**, *37*, 2195–2199.
21. Sun, D.; Hong, X.; Cui, H.; Liu, L. Iterative multi-channel FH-MFSK reception in mobile shallow underwater acoustic channels. *IET Commun.* **2020**, *14*, 838–845. [CrossRef]
22. Tao, Y.; Zhu, P.B.; Xu, X.m. Dual-mode modulation based research of underwater acoustic modem. In Proceedings of the 2010 6th International Conference on Wireless Communications Networking and Mobile Computing (WiCOM), Chengdu, China, 23–25 September 2010; pp. 1–3.
23. Roy, S.; Duman, T.M.; McDonald, V.; Proakis, J.G. High-rate communication for underwater acoustic channels using multiple transmitters and space–time coding: Receiver structures and experimental results. *IEEE J. Ocean. Eng.* **2007**, *32*, 663–688. [CrossRef]
24. Yan, D.; Wang, F.; Wang, S. Research on the output bit error rate of 2DPSK signal based on stochastic resonance theory. *Mod. Phys. Lett. B* **2017**, *31*, 1850069. [CrossRef]
25. Wang, K.; Chen, S.; Liu, C.; Liu, Y.; Xu, Y. Doppler estimation and timing synchronization of underwater acoustic communication based on hyperbolic frequency modulation signal. In Proceedings of the 2015 IEEE 12th International Conference on Networking, Sensing and Control, Taipei, Taiwan, 9–11 April 2015; pp. 75–80.
26. Li, B.; Tong, F.; Zheng, S.; Chen, D. Bit-error rate gradient descent Doppler estimation for underwater acoustic OFDM communication. *Appl. Acoust.* **2021**, *171*, 107557. [CrossRef]
27. Wang, X.; Zheng, S.; Tao, Q.; Zhang, F.; Song, A.; Tong, F. Doppler correction of mobile acoustic communication via adjustable AD sampling rate. In Proceedings of the Thirteenth ACM International Conference on Underwater Networks & Systems, Shenzhen, China, 3–5 December 2018; pp. 1–5.
28. Stamatiou, K.; Casari, P.; Zorzi, M. The throughput of underwater networks: Analysis and validation using a ray tracing simulator. *IEEE Trans. Wirel. Commun.* **2013**, *12*, 1108–1117. [CrossRef]
29. Frosch, R.A. Underwater Sound: Deep-Ocean Propagation: Variations of temperature and pressure have great influence on the propagation of sound in the ocean. *Science* **1964**, *146*, 889–894. [CrossRef] [PubMed]
30. HY1203 Sound Velocity Profiler. Available online: https://www.haiyingmarine.com/en/index.php?a=lists&catid=10 (accessed on 31 January 2017).
31. Li, B.; Tong, F.; Li, J.-H.; Zheng, S.-Y. Cross-correlation quasi-gradient Doppler estimation for underwater acoustic OFDM mobile communications. *Appl. Acoust.* **2022**, *190*, 108640. [CrossRef]
32. Tu, X.; Xu, X.; Song, A. Frequency-Domain Decision Feedback Equalization for Single-Carrier Transmissions in Fast Time-Varying Underwater Acoustic Channels. *IEEE J. Ocean. Eng.* **2020**, *46*, 704–716. [CrossRef]
33. Jiang, W.; Zheng, S.; Zhou, Y.; Tong, F.; Kastner, R. Exploiting time varying sparsity for underwater acoustic communication via dynamic compressed sensing. *J. Acoust. Soc. Am.* **2018**, *143*, 3997–4007. [CrossRef]